An experimental and numerical study of particle-laden coaxial jet flows

A. A. Mostafa and H. C. Mongia
Allison Gas Turbine Division, General Motors Corporation, Indianapolis, IN, USA

V. G. McDonell and G. S. Samuelsen
The Combustion Laboratory, Department of Mechanical Engineering, University of California, Irvine, CA, USA

A detailed experimental and numerical study of the developing region of coaxial jet flows with and without glass beads is performed. A two-component phase/Doppler interferometer is used to measure mean and fluctuating velocity components for each phase and particle-number density. The numerical calculation is based on a stochastic Lagrangian treatment for the particles and a recently proposed two-equation turbulence model for two-phase flows.[1] Results show that the particle-number density profile becomes narrower than the corresponding profile for round jet flow and that the particles attain a uniform velocity across the jet radius. The particles attenuate the level of gas turbulence and increase their anisotropy level. The numerical calculations yield reasonable and encouraging agreement with the measurements.

Keywords: turbulence; modeling; two-phase; coaxial jet; measurements

Introduction

Gas turbine combustor performance and durability are strongly influenced by injector-spray characteristics and the attendant interaction with the combustor's internal flow field. To improve understanding of spray–swirler interaction, we conducted a comprehensive experimental and numerical investigation in a stepwise manner. As a first step, we recently presented a detailed study on the developing region of a single particle-laden axisymmetric jet.[1] As a follow-up, the present study deals with the developing region of unconfined turbulent axisymmetric coaxial jets with and without particles.

A number of investigations have contributed to identifying the general features of single-phase coaxial jet flows.[2–4] Matsumoto *et al.*,[4] Chigier and Beer,[5] and Durao and Whitelaw[6] have provided considerable information on the effect of nozzle conditions—such as nozzle-wall thickness and boundary layers on the inside and outside walls of the nozzle—on jet mixing within the developing region. Others[7,8] have investigated the effect of the jet momentum ratio on the flow field with test configurations in which the radial distance separating the coaxial jets was negligible. The general features of this class of single-phase flows are reasonably well understood. However, the effect of seeding the central jet with particles on the mixing of the developing region should be studied to obtain a first-order simulation of a liquid fuel injector surrounded by an annular jet.

A phase/Doppler interferometry was utilized in the present study to make detailed point measurements for both phases. This instrument is capable of providing simultaneous particle-size and velocity measurements, particle number density, and size–velocity correlation. Radial profiles at seven axial locations downstream of two coaxial jets with and without particles are reported. The measurements include mean and root mean square (rms) velocity components, Reynolds stresses of both phases, and particle-number density.

Address reprint requests to Dr. Mostafa, Textron Lycoming, Stratford, CT 06497, USA.

Received 15 September 1989; accepted 4 December 1989

Our calculations are based on a recently proposed model for two-phase flows. This model is based on a Eulerian formulation for the gas and a stochastic Lagrangian method for the particles. The modeled conservation equations for the mean motion of the gas are supplemented by a two-equation turbulence model for two-phase flows.[9,10] This turbulence model accounts for the additional energy dissipation caused by the particles. The stochastic Lagrangian method considers the effects of both particle inertia and gas turbulence fluctuations on particle motion and interphase transport quantities. The governing equations of the two phases are fully coupled through the mean and fluctuating relative velocities.

Experimental procedure

Test facility

The testing facility shown in Figure 1(a) was designed to characterize a wide variety of flows under isothermal conditions. For the present study, an unconfined flow configuration was selected, operating with an axial jet injector surrounded by a nonswirling annular jet, as shown in Figure 1(b). In this configuration, the injector is directed vertically downward within a 457-mm square wire mesh screen. The pipe extends 59 diameters upstream from the injector to obtain fully developed profiles at the exit plane. The entire test assembly is surrounded by a flexible plastic enclosure, which serves two primary purposes. First, the enclosure helps damp out extraneous room drafts. Second, and most important, the enclosure allows uniform seeding of the entrained air, thereby permitting unbiased measurements in the jet's outer region. Test-section air flows into a sealed collection drum and then into a suction vent connected to an exhaust blower. A slide valve on the vent allows for a variable duct back pressure. The support cage is mounted on an optics table from below by means of a two-axis traverse system, allowing two degrees of freedom horizontally. The injector is mounted on a vertical spar to provide the third degree of freedom—vertically. The control-volume spatial location is monitored through a three-axis digital indicator that permits

positioning to within 0.01 mm. Data were obtained at seven axial stations: 15, 25, 35, 50, 75, 150, and 300 mm from the exit plane of the injector. At each axial station, between 10 and 20 radial points were scanned, as determined by the desired level of profile resolution.

Diagnostics

A two-component phase/Doppler system (Aerometrics, Inc., Model No. 2100-3) was used to map the relevant flow field. This instrument simultaneously measures size and two orthogonal components of velocity for individual particles.[11] The phase/Doppler measurement technique was evaluated against other techniques in a series of studies[12,13] and gave accurate measurements of three components of mean and fluctuating velocities of gas and particles, two cross components of gas-phase Reynolds stresses, particle-size distribution, and particle-number density. Distinguishing between positive and negative flow directions was made possible by frequency shifting provided by the rotating gratings.

Discrimination of phases or of different particle sizes is inherent in the operation of the system[14]. Our approach was to size all scatterers and then use the size measured to discriminate between phases when calculating velocity statistics. Figure 2 shows a typical distribution obtained from measuring the gas phase in the presence of glass beads.

Glass beads

From both the experimental and numerical standpoints, using glass beads with an acceptable quality and size distribution is important. Air classification of the beads was necessary to provide a uniform distribution, as shown in Figure 3. The actual sizes of the air-classified beads, determined by microscopic examination, were between 100 μm and 110 μm. This resulting narrow size range provides for (1) better representation of a monodispersed, nonevaporating spray and (2) better discrimination by the phase/Doppler. Figure 4 shows a typical distribution obtained for two sizes mixed together. Clear separation is evident between the data obtained for each size. Figure 4 shows little deviation in mean velocity within a given size group, indicating that the classification method used is sound.

Data sets

This article presents two data sets for the flow conditions given in Table 1. The center jet ($D=2.41$ cm) is surrounded by an annular jet with inner and outer diameters of 2.9 cm and 3.67 cm, respectively. The effective area ratio and axial velocity ratio of the annular jet to the central jet are 0.87 and 1.4, respectively. To facilitate direct comparison of data and predictions, we present the results graphically. However, the experiment is documented in ref. 15, and data are tabulated following the format outlined in ref. 16.

Mathematical model

The modeled conversion equations for turbulent two-phase flow along with the modeling assumptions are described in a previous publication.[1,10] Therefore we only briefly describe the modeled equations in the following paragraphs. The equations of particle motion are cast in the Lagrangian form; the equations of carrier-phase transport follow the Eulerian treatment. The governing equations of the two phases are coupled primarily by the momentum interchange and the extra energy dissipation owing to the relative velocity fluctuation between the gas and particles.

Notation

$c_\mu, c_{\varepsilon 1}, c_{\varepsilon 2}, c_{\varepsilon 3}$	Coefficients in the turbulence model
C_D	Drag coefficient
d	Particle diameter
D	Inner nozzle diameter ($=2r_o$)
F	Interphase friction coefficient
g	Gravitational acceleration
K	Kinetic energy of turbulence
l_e	Eddy size
m	Particle mass
m	Particle mass flow rate
N	Number of particles represented by the trajectory k
n	Particle-number density
P	Static pressure
r	Distance in the radial direction
Re	Reynolds number
t_i, t_o	The times when the particle enters and leaves the carrier phase control volume
$U, u, \tilde{U}$	Mean, fluctuating, and instantaneous velocity of the carrier phase
$V, v, \tilde{V}$	Mean, fluctuating, and instantaneous velocity of the particles
z	Distance in the axial direction

Greek symbols

ε	Kinetic energy dissipation rate
μ	Dynamic viscosity of the carrier phase
ν_t	Kinematic eddy viscosity of the carrier phase
ρ	Material density
τ_d	Particle dynamic relaxation time
τ_e	Turbulent eddy lifetime
τ_L	Carrier phase Lagrangian time scale
τ_r	Residence time of the particle in the eddy
$\sigma_k, \sigma_\varepsilon$	Coefficients in the turbulence model
Φ	Volume fraction

Subscripts

0	Conditions at the nozzle exit
1	Carrier phase
2	Dispersed phase
c	Conditions at the jet centerline
i	ith direction
r	Radial direction
z	Axial direction
θ	Azimuthal direction

Superscripts

k	kth trajectory of a computational particle

Abbreviations

DT	Deterministic treatment
LR	Mass flow rate of the particles compared with that of air in the inner jet
rms	Root mean square of the velocity fluctuation
ST	Stochastic treatment

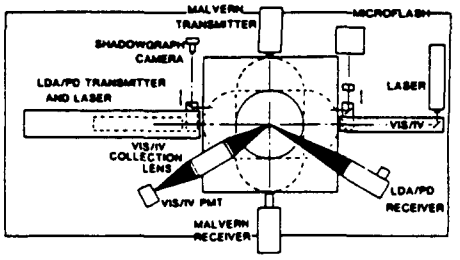

a) Facility

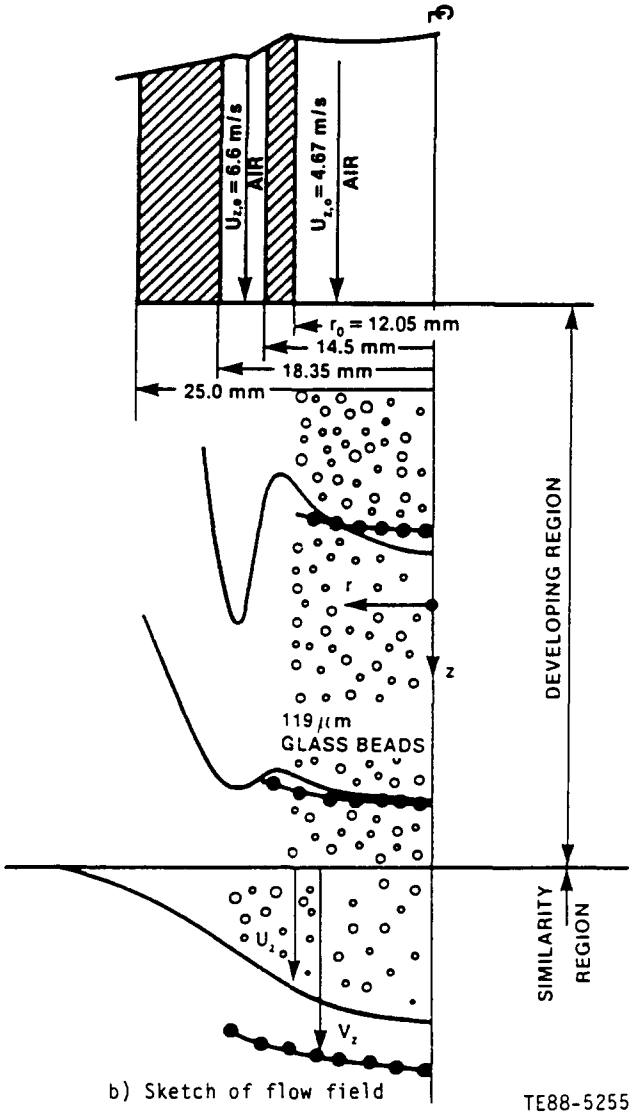

Figure 1 (a) Facility; (b) sketch of flow field

Particle equations

In the discrete particles approach of this study, the dispersed phase is represented by computational particles rather than a continuous distribution function. Each of these computational particles characterizes a group of physical particles possessing the same characteristics, such as size, velocity, and temperature. For a large particle-density to gas-density ratio, the only important forces on a particle are inertia, drag, and gravity, in

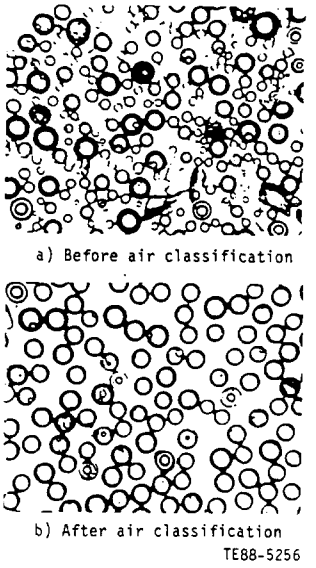

Figure 2 Glass-bead distribution (a) before and (b) after air classification

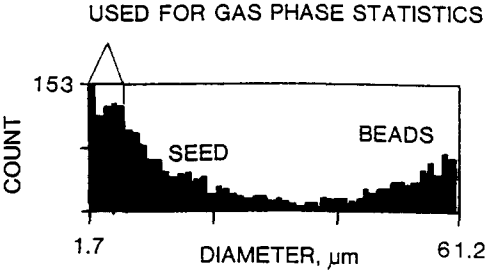

Figure 3 Discrimination of phases based on size-number distribution

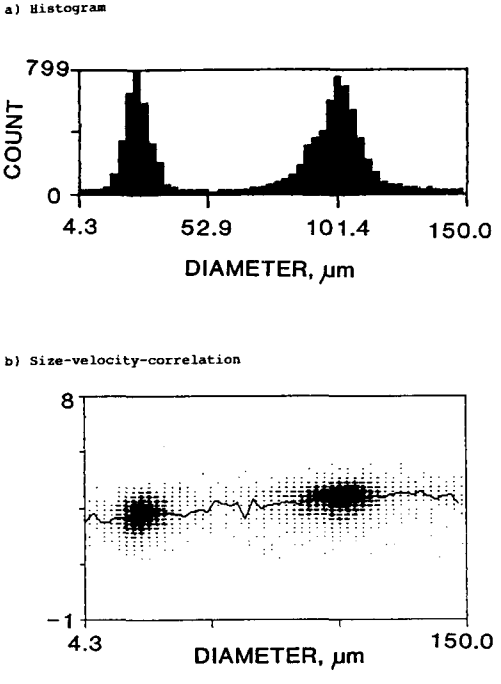

Figure 4 Size class discrimination: (a) histogram; (b) size–velocity correlation

Table 1 Experimental flow conditions at 0.62 D^a downstream of exit plane[b]

Parameter	Single-phase flow	Particle-laden flow	
		Air	Particles
Inner jet			
Centerline velocity, $U_{z,o}$ m/sec	4.64	4.76	4.20
Density, ρ_1 kg/m^3	1.178	1.178	2500.0
Mass flow rate, $\dot{m}_1$ kg/sec	0.0021	0.0021	0.00042
Reynolds number, $\mathrm{Re}=4m_1/\pi\mu_1 D$	6000	6000	
Ratio of particle-to-gas mass flow rate, LR		0.2	
Annular jet			
Maximum velocity, $U_{z,e}$ m/sec	6.60	6.60	
Density, ρ_1 kg/m^3	1.178	1.178	
Mass flow rate, $\dot{m}_2$ kg/sec	0.0033	0.0033	

[a] $D=0.0241$ m.
[b] Inlet profiles of mean and fluctuating velocities and particle-number density are plotted in Figures 3–8

which case the equation of motion of the kth computational particle in the ith direction is

$$\frac{d\tilde{V}_i^k}{dt}=\frac{(\tilde{U}_i-\tilde{V}_i^k)}{\tau_d}+g_i \tag{1}$$

where

$$\tau_d=\frac{4d^k\rho_2}{3C_D\rho_1|\tilde{U}-\tilde{V}^k|} \tag{2}$$

and

$$\tilde{U}_i=U_i+u_i$$

Assuming that the particles are spherical, we can use the experimental results for the drag coefficient of a solid sphere.[17] We determine the particle location at any instant of time from:

$$\frac{dx_i^k}{dt}=V_i^k \tag{3}$$

In Equation 1, U_i is obtained from the solution of the mean flow equations of the carrier phase. Consistent with the use of the K–ε model for the carrier phase, u_i is chosen randomly from an isotropic Gaussian distribution with a mean square deviation of $\frac{2}{3}K$. Subsequently, after each elapsed time equal to the turbulent characteristics time, τ, a new value for u_i is chosen. Thus τ is the minimum of turbulent eddy lifetime and the residence time of the particle in the eddy.[18]

Carrier-phase equations

The modeled mean equations of the carrier phase in the cylindrical coordinates for axisymmetric jet flow are[19]

$$\rho_1 U_{z,z}+\frac{\rho_1}{r}(rU_r)_{,r}=0 \tag{4}$$

$$\rho_1 U_z U_{z,z}+\rho_1 U_r U_{z,r}=-P_{,z}+\frac{1}{r}(\rho_1 r\nu_t U_{z,r})_{,r}-\sum_k \Phi^k F^k(U_z-V_z^k) \tag{5}$$

$$\rho_1 U_z U_{r,z}+\rho_1 U_r U_{r,r}=-P_{,r}-\sum_k \Phi^k F^k(U_r-V_r^k)-\frac{2}{3}\frac{\rho_1}{r}(rK)_{,r} \tag{6}$$

In Equations 4–6, the comma suffix notation indicates differentiation with respect to the spatial coordinates z and r. The kinematic eddy viscosity of the carrier phase is

$$\nu_t=c_\mu\frac{K^2}{\varepsilon} \tag{7}$$

The modeled equations of the turbulence model for two-phase flows are[19]

$$\rho_1 U_z K_{,z}+\rho_1 U_r K_{,r}=\frac{1}{r}\left(\rho_1\frac{\nu_t}{\sigma_k}rK_{,r}\right)_{,r}+\rho_1\nu_t U_{z,r}U_{z,r}-\rho_1\varepsilon-\sum_k 2KF^k\Phi^k\left(1-\frac{\tau_L}{\tau_L+\tau_d}\right) \tag{8}$$

$$\rho_1 U_z\varepsilon_{,z}+\rho_1 U_r\varepsilon_{,r}=\frac{1}{r}\left(\rho_1 r\frac{\nu_t}{\sigma_\varepsilon}\varepsilon_{,r}\right)_{,r}+c_{\varepsilon_1}\frac{\varepsilon}{K}(\rho_1\nu_t U_{z,r}U_{z,r})-c_{\varepsilon_2}\rho_1\frac{\varepsilon^2}{K}-c_{\varepsilon_3}\frac{\varepsilon}{K}\sum_k\left[2KF^k\Phi^k\left(1-\frac{\tau_L}{\tau_L+\tau_d}\right)\right] \tag{9}$$

The carrier-phase Lagrangian time scale is[20]

$$\tau_L=\frac{0.35K}{\varepsilon} \tag{10}$$

The values of the coefficients appearing in Equations 7–10 are $\sigma_k=1.0$, $c_\mu=0.09$, $\sigma_\varepsilon=1.3$, $c_{\varepsilon_1}=1.44$, $c_{\varepsilon_2}=1.92$, and $c_{\varepsilon_3}=2.0$.

Numerical solution

The carrier-phase governing equations are solved numerically using Spalding's parabolic marching finite difference solution procedure.[20] The present calculations were performed using a fine grid with 100 cross-stream grid points and marching step sizes limited by 3% of the current radial grid width or an entrainment increase of 3%, whichever is smaller.

The ordinary differential equations governing particle motion are solved using a second-order finite difference algorithm. Ten thousand particles are used for the stochastic treatment, and two hundred particles are used for the deterministic treatment. The main difference between the two treatments is that the first considers the effect of gas turbulence on particle motion whereas the second ignores it completely.

Results and discussion

The numerical calculations were started at a downstream distance of 0.62 inner nozzle diameter (15 mm from the nozzle exit), where measured profiles for both phases show no reverse

flow behind the nozzle wall. This approach allowed the use of the parabolic code with a very fine grid to obtain an accurate numerical solution. The measured profiles of mean and rms quantities at $z=15$ mm were used as initial conditions. Consistent with the K–ε model, the initial profile for the turbulence energy dissipation rate was obtained from the measured kinetic energy of turbulence, shear stress, and axial velocity gradient.

Single-phase jet

Calculations were made to establish how well the K–ε model performs against the data before introducing two-phase effects. Figure 5 shows a comparison between predictions and measurements of mean axial velocity, kinetic energy of turbulence, K, and shear stress at the various axial stations: $z/D=0.62$ (initial station), 1.04, 1.45, 2.06, 3.10, 6.2, and 12.45. Solid lines refer to the predictions while symbols represent the measurements. As shown, the results are plotted in a dimensionless form versus r/r_o, where r_o is the radius of the inner jet pipe. The axial velocity is normalized by the centerline velocity, $U_{z,o}$, at the initial station, whereas the other variables are appropriately normalized by the local centerline velocity, $U_{z,c}$. Figure 5 shows that the K–ε model yields good overall agreement with measurements; however, the discrepancies are high for the kinetic energy distribution. The underpredicted values of the kinetic energy of turbulence are more obvious in the regions where the flow

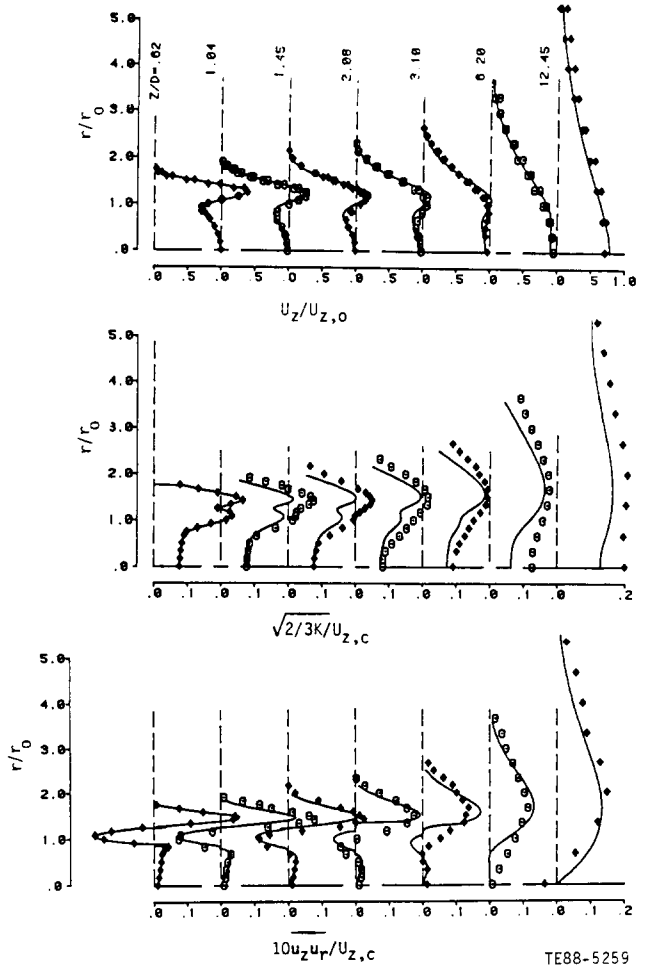

Figure 5 Radial profiles of normalized mean axial velocity, turbulence kinetic energy, and shear stress for the single-phase coaxial jets

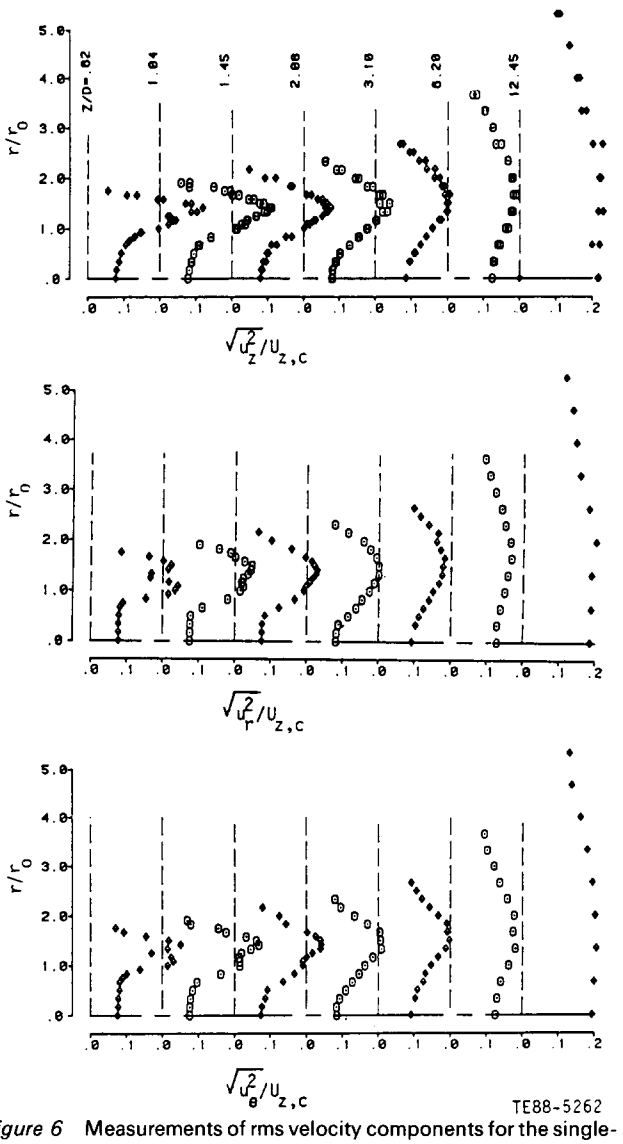

Figure 6 Measurements of rms velocity components for the single-phase coaxial jets

changes rapidly: in the developing shear layer between the two jets (first region) and where the shear layer reaches the centerline (second region).

In the first region, the mixing layer between the two flows produced by the inner and outer streams is changing from a thin layer characterized by a high shear stress to a self-similar shear flow where the shear stress is relatively small. In both regions, the flow possesses two significant rate-of-strain components resulting from the velocity gradients in both the axial and radial directions. This type of flow is classified as complex shear flow, which is difficult to predict by using the standard version of the K–ε model.

The distribution of the turbulent shear stress and its dependence on the mean velocity gradient is also shown in Figure 5. According to the eddy-viscosity hypothesis, the sign of the shear stress and the velocity gradient is clearly consistent across the flow field. The positive shear stress in the inner jet region indicates that the flow still bears the characteristics of the upstream pipe flow; the gradient of mean axial velocity is still negative but approaching zero. The distributions of K and $\overline{u_z u_r}$ reach their more familiar shapes (as in a single free jet) when the mixing takes place across the entire flow and the mean axial velocity gradient becomes negative across the entire jet.

Figure 6 presents the experimental data of the three rms velocity components at the different axial locations. The shapes of the three components have maximum values just behind the nozzle wall and minimum values at the central axis. But in the farther downstream region where the mixing layer merges with the central axis, the rms profiles take a uniform shape like that observed in fully developed jet flows. Figure 6 also shows that the radial rms velocity component, u_r^2, has almost the same value of the axial component.

Particle-laden jets

The mass loading, defined as the ratio of particle-to-gas mass flow rate of the inner jet at the inlet plane, $LR=0.2$, was considered. To distinguish between the effects of mean and fluctuating gas velocity on particle transport, we compared predictions using stochastic and deterministic treatments to the measured data.

Figure 7 presents the mean axial velocity, kinetic energy, and shear stress of the carrier phase. The high velocity of the external stream (compared to that of the central jet) causes a rapid increase in the axial velocity of the inner jet downstream of the exit plant. Because of this transfer of mass and momentum from the external to the internal stream, the carrier-phase velocity distribution where the particles exist, becomes different from that of the axisymmetric jet flow case observed by Mostafa

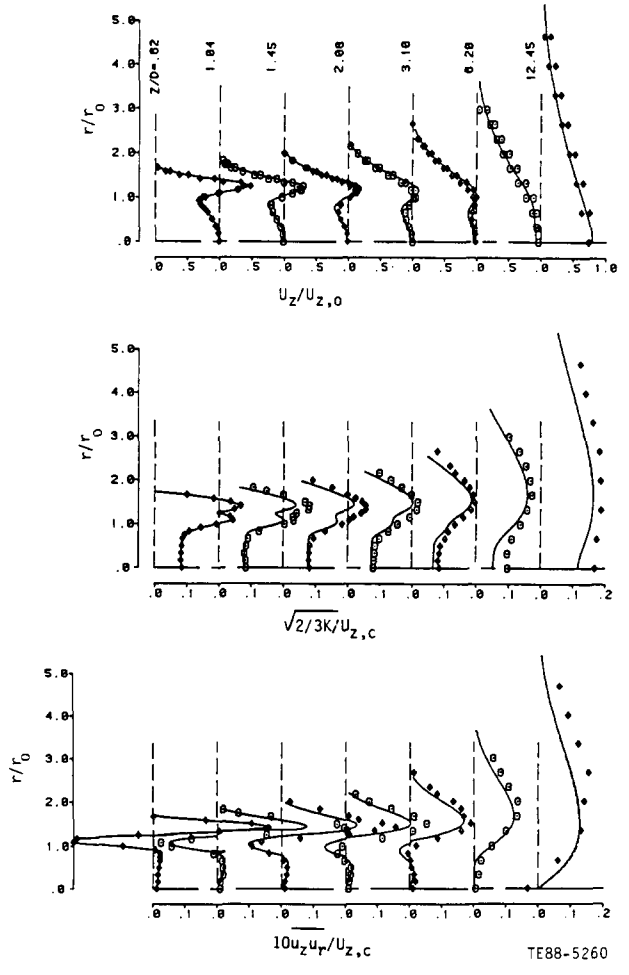

Figure 7 Radial profiles of normalized mean axial velocity, turbulence kinetic energy, and shear stress for the particle-laden coaxial jets

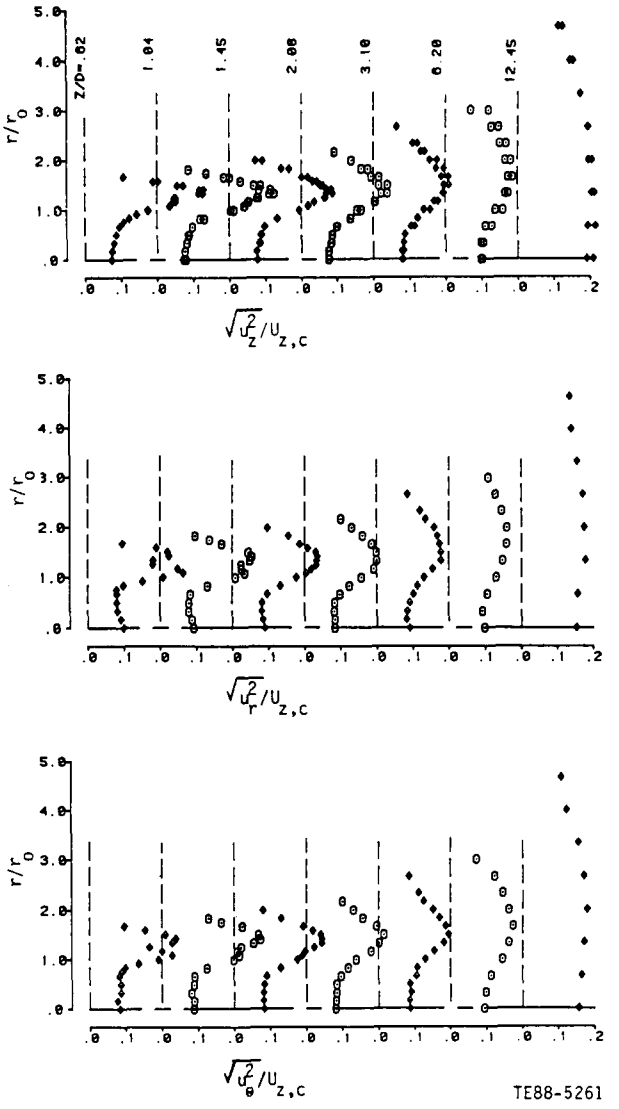

Figure 8 Measurements of rms gas-velocity component for the particle-laden coaxial jets

et al.[1] This change in air velocity affects particle velocity, which we discuss in connection with Figure 7.

The present particle loading is fairly small in terms of altering the carrier-phase flow field.[19] However, comparison of the last two planes in Figure 7 with those of Figure 5 shows some reductions in turbulence kinetic energy and shear stress in the near centerline region where the particles exist. This turbulence modulation is caused mainly by the fluctuating relative velocity between the particles and the carrier phase. Particles generally cause a reduction in gas turbulence and an increase in the dissipation rate of that energy. This phenomenon was simulated in the present study by introducing extra terms into the turbulence kinetic energy and its dissipation rate equations. Increasing the particle loading increases the turbulence modulation, as pointed out by Mostafa *et al.*[1] and recently measured by Fleckhaus *et al.*[21] Figure 7 shows that the present mathematical model yields fairly good agreement with the experimental data.

Figure 8 presents the measured values of the three components of fluctuating velocity of the carrier phase when glass beads are present. The effect of the particles on the radial and azimuthal components is higher than that on the axial component. This condition may be attributed to the differences in the mean

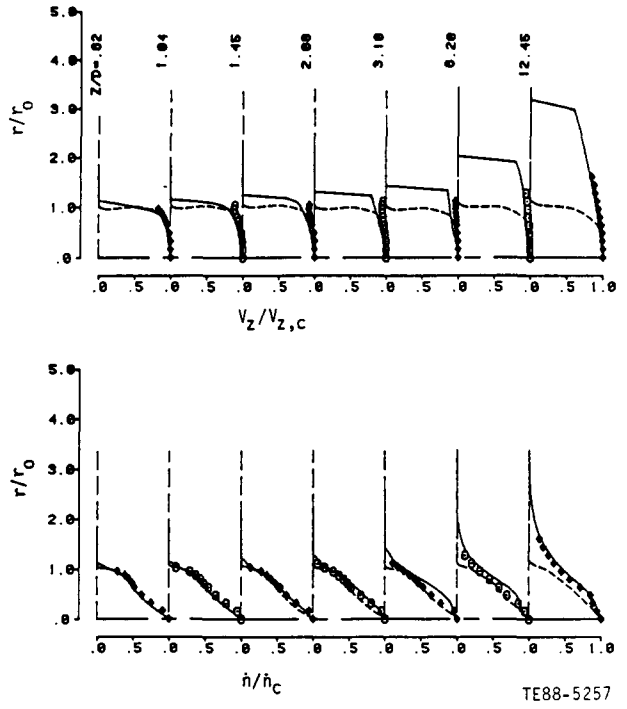

Figure 9 Radial profiles of normalized particle axial velocity and particle-number density: —— stochastic; ---- deterministic

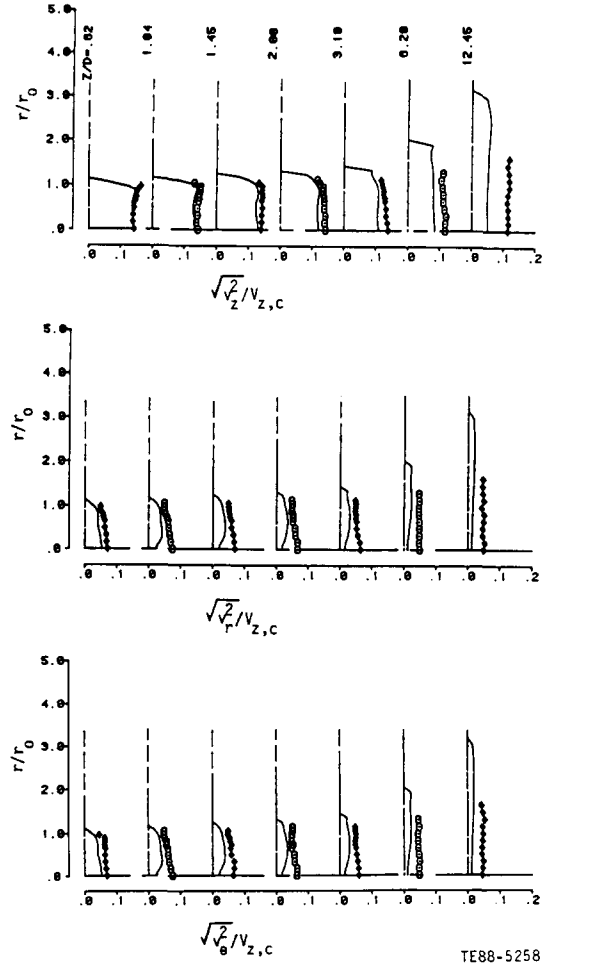

Figure 10 Radial profiles of rms of particle-velocity components

velocity strain profiles and to the small ratio of v_r^2/u_r^2 compared to v_z^2/u_z^2. According to Fleckhaus *et al.*,[21] the smaller the ratio of particle to gas velocity fluctuation, the higher is turbulence attenuation. This observation supports the postulate that particles increase the level of anisotropy and shows the need for detailed measurements of mean and fluctuating components of the two phases under different flow conditions.

Figure 9 presents the data of the mean axial particle velocity and number density. It also compares the predictions of the stochastic (ST) and deterministic (DT) treatments to the experimental data. The mean particle velocity profile is uniform over the entire cross section of the flow field. This behavior is different from that observed in round jet flow measurements[1] and could be attributed to rapid mixing between inner and outer jets, which subjects the particles to a more uniform gas-velocity distribution. This jet mixing process creates a strong negative radial velocity in the jet's outer region and causes the particle-number density to become narrower than the corresponding profile for axisymmetric round jet flows.[1] Figure 9 also shows that the ST provides good predictions, compared to the experimental data, whereas the DT performs quite poorly at the downstream stations. That is, a particle moves radially because of its initial mean radial velocity and/or the mean radial gas velocity, both of which are very small compared to the axial component. This effect explains the narrow distribution of particle mean axial velocity and number density predicted by DT.

Figure 10 presents the measurements of the three components of fluctuating particle velocity and indicates the extent to which ST allows reasonable calculations. Although DT ignores these components entirely, ST simulates these particle-velocity fluctuations as a response to the carrier-phase components. The agreement between predictions and data is less than satisfactory at the last station, which could be attributed to the limitations of the assumptions embedded in the ST's formulation. Figure 10 also shows the high anisotropy of particle turbulent quantities that increase the anisotropy level of the carrier phase discussed in the analysis of Figure 8.

Conclusions

A detailed data set was presented for gas and particle mean and fluctuating velocity and particle-number density within the developing region of particle-laden coaxial jets with 105 μm glass beads. Because of the mixing between inner and outer gas streams, the mean particle velocity becomes uniform over the entire cross section, and the particle-number density profile becomes narrower than the corresponding profile for axisymmetric round jet flows. The presence of the glass beads attenuates the level of the gas turbulence quantities and increases their level of anisotropy. The computations—using the stochastic treatment in conjunction with the recently developed two-phase turbulence model—yield reasonably good agreement with the data.

Acknowledgments

This work was supported, in part, by NASA contract NAS3-24350 (J. D. Holdeman, contract monitor). The participation of Howard C. Crum, Russell W. Benson, and Gil D. Cameron in the collection and analysis of the experimental data is gratefully acknowledged.

References

1 Mostafa, A. A., Mongia, H. C., McDonell, V. G., and Samuelsen, G. S. On the evolution of particle-laden jet flows: A theoretical and experimental study. *AIAA Journal*, **27**, 167–183 1988

2 Habib, M. A. and Whitelaw, J. H. Velocity characteristics of confined coaxial jet with and without swirl. *J. Fluids Eng.*, 1980, **102**, 47–53

3 Forstall, W. and Shapiro, J. H. Turbulent mixing in the developing region of coaxial jets. *J. Fluids Eng.*, 1973, **17**, 399–408

4 Matsumoto, R., Kimoto, K., and Tscichmoto, N. A study of double concentric jets. *Bull. JSME*, 1973, **16**(93), 529–540

5 Chigier, N. A. and Beer, J. M. The flow region near the nozzle in double concentric jets. *ASME J. Basic Eng.*, 1964, **86**, 797–804

6 Durao, D. and Whitelaw, J. H. Turbulent mixing in the developing region of coaxial jets. *J. Fluids Eng.*, 1973, **25**, 467–473

7 Owen, F. K. Laser velocimeter measurements in free and confined coaxial jets with recirculation. AIAA Paper 75-120, Pasadena, CA, 1975

8 Champagne, F. H. and Wygnanski, I. Coaxial turbulent jets. Boeing Scientific Research Laboratories, D1-82-0958, 1970

9 Mostafa, A. A. and Elghobashi, S. E. A two equation turbulence model for jet flows laden with vaporizing droplets. *Int. J. Multiphase Flow*, 1985, **11**, 515–533

10 Mostafa, A. A. and Mongia, H. C. On the modeling of turbulent evaporating sprays: Eulerian versus Lagrangian approach. *Int. J. Heat Mass Transfer*, 1987, **30**, 2583–2593

11 Bachalo, W. D. and Houser, M. J. Phase/Doppler spray analyzer for simultaneous measurements of drop size and velocity distributions. *Opt. Eng.*, 1984, **23**(5), 583–590

12 Jackson, T. A. and Samuelsen, G. S. Droplet sizing interferometry: A comparison of the visibility and phase Doppler techniques. *Appl. Opt.*, 1987, **26**, 2137–2143

13 McDonell, V. G., Wood, C. P., and Samuelsen, G. S. A comparison of spatially-resolved drop size and drop velocity measurements in an isothermal chamber and swirl-stabilizing combustor. *Proc. of the Twenty-First Symposium (Int.) on Combustion*. The Combustion Institute, Pittsburgh, PA, 1987, 685

14 Alexander, D. R., Wiles, K. J., Schaub, S. A., and Seeman, M. P. Effects of nonspherical drops on a phase Doppler spray analyzer. *SPEI Conference Proceedings*, vol. 573. Society of Photo-Optical Instrumentation Engineers, Bellingham, WA, 1985

15 McDonell, V. G. and Samuelsen, G. S. Detailed data set: Two-component gas and particle velocity statistics in a particle-laden jet flow. UCI Combustion Laboratory Report ARTR 87-1, Department of Mechanical Engineering, University of California, Irvine, CA, 1987

16 Faeth, G. M. and Samuelsen, G. S. Fast reaction nonpremixed combustion. *Progress in Energy and Combustion Science*, 1987, **12**(4), 341–372

17 Clift, R., Grace, J. R., and Weber, M. E. *Bubbles, Drops, and Particles*. Academic Press, New York, 1978

18 Gosman, A. D. and Ioannides, E. Aspects of computer simulation of liquid fueled combustors. *AIAA J. Energy*, 1983, **7**, 482–490

19 Mostafa, A. A. and Mongia, H. C. On the interaction of particles and turbulent fluid flow. *Int. J. Heat Mass Transfer*, **31**, 2063–2075 1988

20 Spalding, D. B. *GENMIX: A General Computer Program for Two-Dimensional Parabolic Phenomena*. Pergamon Press, Oxford, 1978

21 Fleckhaus, D., Hishida, K., and Maeda, M. Effect of laden solid particles on the turbulent flow structure of a round free jet. *Experiments in Fluids*, 1987, **5**, 323–333